Fiber Bragg Grating Based Needle Shape Sensing for Needle Steering System: Evaluation in Inhomogeneous Tissue

Jin Seob Kim*, Maria Chatrasingh†, Sungmin Kim‡, Jackrit Suthakorn† and Iulian I. Iordachita*
*Department of Mechanical Engineering, Johns Hopkins University, Baltimore, MD, USA
Email: {jkim115,iordachita}@jhu.edu
†Department of Biomedical Engineering, Mahidol University, Bangkok, Thailand
Email: maria@bartlab.org, jackrit.sut@mahidol.ac.th
‡Department of Computer Science, Johns Hopkins University, Baltimore, MD, USA
Email: sungminkim@jhu.edu

***Abstract*—Despite many successful studies so far, flexible bevel-tipped needle steering still has many practical issues yet to be solved. One of them is the consideration of needle insertion into real tissue. One notable feature of real tissue lies in its inhomogeneity. Hence the investigation of flexible needle insertion into inhomogeneous tissue is necessary. In this work, we examine the flexible needle insertion into three-layered phantom tissue. In particular, needle shape determination is executed by the method that was proposed previously, which combines a novel model that treats the needle as an inextensible elastic rod and curvature measurement through fiber Bragg grating (FBG) sensors embedded in the needle. Experiments on needle insertion into three-layered tissue are performed, then we evaluate the method. The results emphasize the effectiveness of the model and importance of initial angle in the needle insertion into tissues of different material properties.**

***keywords*—flexible needle; FBG; mathematical model; tissue inhomogeneity;**

I. Introduction

Needle insertion is common practice in clinical intervention for injection, biopsy, or brachytherapy. Flexible needles with asymmetric bevel tips are a conventional design to decrease tissue damage and its consequences. The bevel tip causes the needle's trajectory to deviate from a straight line path, hence requires physicians to steer the needle by bending it back toward the designated target.

Flexible needle insertion conventionally requires real-time imaging techniques such as ultrasound imaging (US) [1] and magnetic resonance imaging (MRI) [2] to monitor needles trajectory. Another choice of measurement techniques includes fiber Bragg grating (FBG) sensors embedded into the flexible needle. This technique integrates the optic fiber strain gauge into specific locations of the needle hence provides the real-time bending curvature of the needle at the locations [3]. One notable feature of FBG sensors is MR-compatibility [4]. Hence, an FBG-based needle can be used together with the aforementioned imaging techniques. As well as measurement techniques, a needle model is necessary for a better control and planning of the needle. For this reason, several mathematical models for needle steering have been developed for preoperative needle steering path planning [5]–[7].

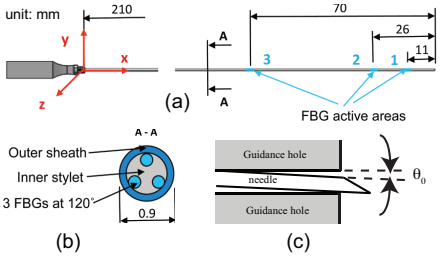

Fig. 1. (a) Design of FBG-based sensorized needle. (b) Cross-section of the needle. (c) Initial rotation angle θ_0.

Another important issue comes from the consideration of needle insertion into real tissue. One notable feature of real tissue lies in its inhomogeneity. Hence the investigation of flexible needle insertion into inhomogeneous tissue is necessary. Recent modeling effort tried to address this issue by considering needle insertion into double-layered phantom and real porcine tissue (skin and muscle layer) [8].

In this paper we evaluate the mathematical model for needle shape sensing developed by Kim, et al. [9] in conjunction with an FBG-based bevel-tipped needle during insertion into inhomogeneous tissue. The model is based on the general elastic rod theory and Lie-group-theoretic approach, of which one advantage is its ability to compute out-of-plane deformation and torsional deformation that are presumably small yet possible during needle insertion without rotation. The model has already been evaluated during needle insertion in homogeneous and double-layered phantoms [9] where the results ensure the effectiveness in terms of shape prediction. In this paper, we examine the flexible needle insertion into three-layered phantom tissue. The test phantom consists of three layered soft materials; soft gel (Super soft plastic from M-F Manufacturing Company, TX, US) layer, meat (beef) layer, and soft gel layer, respectively. The meat layer represents the biological tissue in which the materials properties are unknown and homogeneity could not be guaranteed. In addition, we discuss an important factor for predicting correctly the needle deflection (position), namely the initial rotation angle (θ_0) about the x-axis at the insertion point (Fig. 1 (c)).

978-1-5090-1012-7/17/$31.00 ©2017 IEEE

II. The Model

The model (see [9] for the details) uses Lie-group theory approach to explain the curvature of the needle as an inextensible elastic rod, which is expressed as

$$\boldsymbol{\omega}(s) = [\omega_1 \ \omega_2 \ \omega_3]^T = \left(R(s)\frac{dR(s)}{ds}\right)^{\vee} \tag{1}$$

where $R(s) \in SO(3)$ denotes the rotation matrix in 3D space which describes the orientation of the body-fixed frame attached at each point along the needle. $s \in [0, L]$ denotes the arclength of the needle with total insertion length L. Here $\vee$ operation defines a vector, expressed in the body-fixed frame, associated with a 3×3 skew-symmetric matrix $R^T \frac{dR}{ds}$ [10]. Note that ω_1 and ω_2 denote the curvature along the local x- and y-axes, whereas ω_3 denotes the torsion along the local z-axis.

When inserting into the three layered phantom, the needle is modeled as an inextensible elastic rod. In the ideal case of needle insertion into three-layered tissue, we can assume that the needle is under three different distributed loads for different portions of its arclength. Hence, the needle will bend only in one plane (yz plane), which can be effectively captured by introducing the intrinsic curvature $\kappa_0(s)$. Inspired by the classical beam theory with uniform loads, we propose the form of $\kappa_0(s)$ as

$$\kappa_0(s) = \begin{cases} \kappa_{c,1}\left(\frac{s_1^*-s}{L}\right)^2 + \kappa_{c,2}\left(\frac{s_2^*-s_1^*}{L}\right)\left(\frac{s_2^*+s_1^*-2s}{L}\right) \\ \quad +\kappa_{c,3}\left(1-\frac{s_2^*}{L}\right)\left(1+\frac{s_2^*-2s}{L}\right) \ (0 \le s \le s_1^*) \\ \kappa_{c,2}\left(\frac{s_2^*-s}{L}\right)^2 + \kappa_{c,3}\left(1-\frac{s_2^*}{L}\right)\left(1+\frac{s_2^*}{L}-\frac{2s}{L}\right) \\ \qquad\qquad (s_1^* \le s \le s_2^*) \\ \kappa_{c,3}\left(1-\frac{s}{L}\right)^2 \ (s_2^* \le s \le L) \end{cases} \tag{2}$$

where $\kappa_{c,1}$, $\kappa_{c,2}$ and $\kappa_{c,3}$ are curvature parameters for material 1, 2, and 3, respectively. s_1^* and s_2^* are the arclengths of the needle corresponding to the first boundary and second boundary between layers (Fig. 2). These values are approximately determined as: first, compute the needle shape assuming one layer and two layers. Then calculate z-coordinates and compare with the widths of the boundaries to select the corresponding arclength points which gives s^*'s. This intrinsic curvature is important in the model in that it provides a reference to which the actual needle deformation will follow. The elastic potential energy of the needle then can be written as

$$\mathcal{V} = \int_0^L \frac{1}{2}\left(\boldsymbol{\omega}-\boldsymbol{\omega}_0\right)^T B\left(\boldsymbol{\omega}-\boldsymbol{\omega}_0\right) ds \tag{3}$$

where B is stiffness matrix of the needle including the bending and torsional stiffnesses, and $\boldsymbol{\omega}_0 = [\kappa_0 \ 0 \ 0]^T$. Minimizing this potential energy allows us to find the actual needle deformation $\boldsymbol{\omega}(s)$ and the body-fixed frame $R(s)$ along the needle shaft. Specifically, the minimization of the equation gives the Euler-Poincaré equation [11], [12] as

$$\frac{d}{ds}\left[B\left(\boldsymbol{\omega}-\boldsymbol{\omega}_0\right)\right] + \boldsymbol{\omega} \times B\left(\boldsymbol{\omega}-\boldsymbol{\omega}_0\right) = \mathbf{0} \tag{4}$$

which will be solved together with (1). Then the position of the points along the needle, $\mathbf{r}(s)$, can be determined as

$$\mathbf{r}(s) = \int_0^s R(\sigma)\mathbf{e}_3 \, d\sigma \tag{5}$$

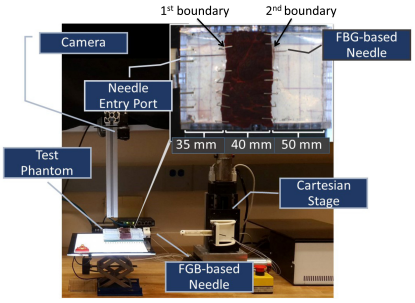

Fig. 2. Experimental setup and top-view of the three-layered phantom tissue.

where $\mathbf{e}_3 = [0 \ 0 \ 1]^T$.

Finally, this approach is combined with FBG sensor reading to optimize the following cost function

$$\mathcal{C}(\boldsymbol{\eta}) = \sum_{j=1}^{m}\left\{\left(\omega_{j,1}^{\mathrm{m}} - \omega_1(s_j)\right)^2 + \left(\omega_{j,2}^{\mathrm{m}} - \omega_2(s_j)\right)^2\right\} \tag{6}$$

where $\omega_{j,1}^{\mathrm{m}}$ and $\omega_{j,2}^{\mathrm{m}}$ denote the curvature data from the FBGs (m is the number of FBGs). An array of optimization variables, $\boldsymbol{\eta}$, includes the initial value of $\boldsymbol{\omega}$ (for integrating (4)) and $\kappa_{c,i}$ ($i = 1, 2, 3$). In theory, we have to include all three $\kappa_{c,i}$ ($i = 1, 2, 3$) in the optimization process which would result in better accuracy, but in this work, we only include that of the meat layer ($\kappa_{c,2}$) in the optimization, and use the values of $\kappa_{c,i}$ ($i = 1, 3$) obtained from the soft-gel homogeneous tissue needle insertion.

III. Experiments

A. FBG-based sensorized needle

We have developed an in-house FBG-based sensorized needle [3] where FBG sensors are located at 11, 26, and 70 mm from its tip as shown in Fig. 1 (a). Fig. 1 (b) illustrates the cross-sectional area of the FBG-sensorized needle, where three optical fibers are attached inside the needle. Details on the experimental setup and FBG sensors can be found in [9].

B. Needle insertion into three-layered tissue

We evaluated the model on homogeneous material, single- and double-layered phantoms in [9]. In this paper, the goal is to verify the effectiveness of the model during insertion in inhomogeneous materials through needle insertion into three-layered phantom.

The phantom consists of three layers; soft gel-meat-soft gel, width size of 35mm, 40mm, and 50 mm, respectively. The needle was inserted into the phantom in five different entry ports, at 0 and 180 degree axial rotation to account for material inhomogeneity. In total 10 insertions were performed. The corresponding FBGs wavelength shifts at 90 mm arclength insertion were transformed to the curvatures at three different locations along needle using 'jig' and 'beam' calibration methods [9]. The needle shapes by 90 mm insertion were extracted using the corresponding calibrated image as ground truth (see [9] for the detailed explanation). The efficiency of the model was compared to the 4th order polynomial interpolation method [3].

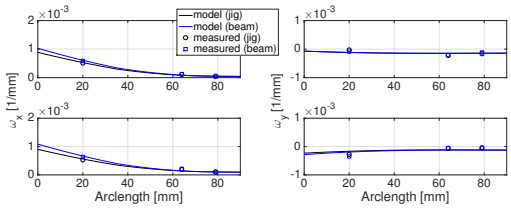

Fig. 3. Selected plots of the needle deformation. Left-column plots show ω_x. In the right column, plots are for ω_y.

TABLE I. STATISTICS (MEAN $\pm$ STD) FOR SOFT GEL-BEEF- SOFT GEL PHANTOM EXPERIMENT COMPARE BETWEEN ADOPTING θ_0 AS CONSTANT AND θ_0 AS AN OPTIMIZED VARIABLE.

	Using constant θ_0		Using θ_0 optimization	
	RMSE [mm]	Tip Defl [mm]	RMSE [mm]	Tip Defl [mm]
Model (jig)	0.22 ± 0.15	0.31 ± 0.26	0.13 ± 0.06	0.18 ± 0.13
Model (beam)	0.22 ± 0.17	0.38 ± 0.27	0.14 ± 0.06	0.18 ± 0.14
Interpolation	0.21 ± 0.15	0.30 ± 0.31	0.13 ± 0.07	0.17 ± 0.12

IV. RESULTS

First, the model could generate the profile of needle deformation as in Fig. 3. In Fig. 3, the plots in the left and right columns respectively show the curvature along the local x- and y-axis, ω_x and ω_y, all of which show excellent agreements between the model results and measurement data.

Next, we consider the needle trajectories. The accuracy of needle shape determination was evaluated via root mean square method (RMSE) and tip deflection error (Tip Defl), as shown in Table I. In determining the needle shape, the so-called "initial rotation angle" θ_0 (Fig. 1 (c)), due to misalignment of the needle and the guidance hole, is important. This angle is currently not possible to measure due to the limitation of image resolution. Previous work used additional optimization on θ_0, which showed that the results were in good agreements with a simple estimate (about 1° from geometrical consideration) [9]. Here we considered two cases (i.e., using constant θ_0 and performing additional optimization on θ_0) to verify the previous conclusion is still valid. Specifically, constant θ_0 value for the former is obtained by taking a mean value of θ_0's from optimization results (see Table II).

Considering that the model used previously obtained κ_c values for the soft-gel layer, the model results show similarly excellent accuracy with the published method, which emphasizes the effectiveness of the model. Noting that the error of image analysis is about 0.2 mm, all the results can be considered very accurate. Of importance is the effect of θ_0, which is immeasurable by the FBGs. Compared with homogeneous tissue cases, three-layered cases have smaller values of θ_0 in Table II, which suggests that θ_0 depends not only on the 1st layer but also on the 2nd layer; especially when the second layers stiffness is relatively high (as in the current 3 layered situation). It might cause further needle deformation as the needle passes through the stiffer layer, as inferred from lower θ_0 than single-layered tissue cases in Table II.

V. CONCLUSION

We applied the method that was previously proposed to three-layered phantom (soft gel-meat-soft gel) which mimics inhomogeneous real tissue. The use of a three-layers phantom is an important step forward in the assessment of the model and the system close to a clinical scenario. By comparing the model and the experimental results, the model can determine the needle shape accurately, which emphasizes the effectiveness of the model. Furthermore, we emphasized the importance of the initial rotation angle θ_0 in needle shape determination: θ_0 is shown to depend on layers' properties. Also consideration on more complex needle insertion and 3D measurement of needle trajectories are not included in the current study. All these form our future research endeavors.

TABLE II. STATISTICS (MEAN $\pm$ STD) OF OPTIMIZED θ_0 THE FOR HOMOGENEOUS [9] AND THREE-LAYERED PHANTOMS

	Homogeneous ($^\circ$)	Three-layered ($^\circ$)
Model (jig)	1.34 ± 0.36	0.45 ± 0.34
Model (beam)	1.06 ± 0.34	0.31 ± 0.34
Interpolation	1.50 ± 0.36	0.63 ± 0.36

ACKNOWLEDGMENT

This work has been supported by Johns Hopkins University internal funds and by the National Institute of Health under grant No. R01CA111288.

REFERENCES

[1] T. K. Adebar, A. E. Fletcher, and A. M. Okamura, "3D ultrasound-guided robotic needle steering in biological tissue," *IEEE Transactions on Biomedical Engineering*, vol. 61, no. 12, pp. 2899–2910, 2014.

[2] R. Seifabadi, E. E. Gomez, F. Aalamifar, G. Fichtinger, and I. Iordachita, "Real-time tracking of a bevel-tip needle with varying insertion depth: Toward teleoperated MRI-guided needle steering," *IEEE International Conference on Intelligent Robots and Systems*, pp. 469–476, 2013.

[3] M. Li, G. Li, B. Gonenc, X. Duan, and I. Iordachita, "Towards human-controlled, real-time shape sensing based flexible needle steering for MRI-guided percutaneous therapies," *Int. J. Med. Robotics Comput. Assist. Surg.*, 2016.

[4] F. Taffoni, D. Formica, P. Saccomandi, G. Di Pino, and E. Schena, "Optical fiber-based MR-compatible sensors for medical applications: an overview," *Sensors*, vol. 13, no. 10, pp. 14 105–14 120, 2013.

[5] R. J. Webster III, J. S. Kim, N. J. Cowan, G. S. Chirikjian, and A. M. Okamura, "Nonholonomic modeling of needle steering," *Int. J. of Robot. Res.*, vol. 25, no. 5–6, pp. 509–525, 2006.

[6] S. P. Dimaio and S. E. Salcudean, "Needle steering and motion planning in soft tissues," *IEEE Transactions on Biomedical Engineering*, vol. 52, no. 6, pp. 965–974, 2005.

[7] M. Khadem, B. Fallahi, C. Rossa, R. S. Sloboda, N. Usmani, and M. Tavakoli, "A mechanics-based model for simulation and control of flexible needle insertion in soft tissue," in *Proceedings of IEEE International Conference on Robotics and Automation (ICRA)*, Seattle, Washington, May 26–30 2015, pp. 2264–2269.

[8] H. Lee and J. Kim, "Estimation of flexible needle deflection in layered soft tissues with different elastic moduli," *Med. Biol. Eng. Comput.*, vol. 52, no. 9, pp. 729–740, 2014.

[9] J. Kim, J. Guo, M. Chatrasingh, S. Kim, and I. Iordachita, "Shape determination during needle insertion with curvature measurements," in *IEEE/RSJ International Conference on Intelligent Robots and Systems (IROS)*, 2017 (accepted).

[10] G. Chirikjian and A. Kyatkin, *Harmonic Analysis for Engineers and Applied Scientists*. Dover, September 2015, (updated and expanded version of Engineering Applications of Noncommutative Harmonic Analysis, CRC Press, October 2000.).

[11] D. D. Holm, J. E. Marsden, and T. S. Ratiu, "The Euler-Poincaré equations and semidirect products with applications to continuum theories," *Advances in Mathematics*, vol. 137, pp. 1–81, 1998.

[12] J. S. Kim and G. S. Chirikjian, "Conformational analysis of stiff chiral polymers with end-constraints," *Molecular Simulation*, vol. 32, pp. 1139 – 1154, 2006.